

# Novel *In-Situ* SEI Fabrication on Zn Anodes for Ultra-High Current Density Tolerance Enabled by Electrical Excitation-Conjugation of Iminoacetonitrile

Ruqian Zhang<sup>1, #</sup>, Tao Shui<sup>1, #, \*</sup>, An Li<sup>2</sup>, Huan Xia<sup>1</sup>, Gang Xu<sup>1</sup>, Lingfeng Ji<sup>1</sup>, Chengjie Lu<sup>1, \*</sup>, Wei Zhang<sup>1, \*</sup>, ZhengMing Sun<sup>1, \*</sup>

<sup>1</sup> School of Materials Science and Engineering, Southeast University, Nanjing, 211189, P. R. China.

<sup>2</sup> Analysis and Testing Center, Southeast University, Nanjing, 211189, P. R. China.

\*Corresponding authors: tshui@seu.edu.cn; lucj008@126.com; w69zhang@seu.edu.cn;  
zmsun@seu.edu.cn

# These authors contribute equally to this work

## Experimental Section

### Materials

Zinc foil (10, 20 and 100  $\mu\text{m}$ ), copper foil (50  $\mu\text{m}$ ) and titanium foil (50  $\mu\text{m}$ ) were purchased from Shengshida, Hebei province. Stainless steel mesh (500 mesh) and aluminum plastic film were purchased from Saibo. Glass fiber (GF/D) was purchased from Whatman. Coin cells (CR 2032) was purchased from Beike. Super P and polyvinylidene difluoride (PVDF) were purchased from Modges, Nanjing. Iminodiacetonitrile (IDAN, 98%) was purchased from TCI.  $\text{Zn}(\text{OTf})_2$  (98%) was purchased from Sigma-Aldrich.  $\text{ZnSO}_4 \cdot 7\text{H}_2\text{O}$  (AR, 99.5%),  $\text{Zn}(\text{ClO}_4)_2 \cdot 6\text{H}_2\text{O}$  (99.995%),  $\text{ZnCl}_2$  (99.95%),  $\text{Na}_2\text{SO}_4$  (AR, 99%),  $\text{NH}_4\text{VO}_3$  (99%),  $\text{H}_2\text{C}_2\text{O}_4 \cdot 2\text{H}_2\text{O}$  (99%), 1-Methyl-2-pyrrolidinone (NMP, 99.9%) and Nessler's agents were all purchased from Aladdin, Shanghai.

### Experimental Methods

#### Preparation of Zn@IIS

First, 57.5 g of  $\text{ZnSO}_4 \cdot 7\text{H}_2\text{O}$  was dissolved in 100 mL of deionized water to

prepare a 2 M ZnSO<sub>4</sub> solution. IDAN at a concentration of 5.0 g·L<sup>-1</sup> was then added to the 2 M ZnSO<sub>4</sub> solution to form the electroplating solution. Following this, the stamped zinc foils were immersed in the electroplating solution and assembled into a homemade Zn||Zn electrolytic cell for electroplating (50 mA·cm<sup>-2</sup>, 120 s). Finally, the Zn@IIS was obtained from the discharged zinc electrode.

### Preparation of Other Electrodes

Copper and titanium foils were stamped into discs ( $\phi = 10$  mm) to be used as copper and titanium electrodes. Zinc foils were ultrasonically cleaned with ethanol and polished with sandpaper to remove the passivation layer. The cleaned zinc foils were then stamped into discs ( $\phi = 10$  mm) to be used as zinc anodes.

Ammonium vanadate (NH<sub>4</sub>V<sub>4</sub>O<sub>10</sub>) was synthesized via a hydrothermal method.<sup>[1]</sup> Typically, 1.170 g of ammonium metavanadate (NH<sub>4</sub>VO<sub>3</sub>) was dissolved in 70 mL of deionized water and stirred at room temperature for 10 minutes. Subsequently, 1.891 g of oxalic acid (H<sub>2</sub>C<sub>2</sub>O<sub>4</sub>·2H<sub>2</sub>O) was added to this solution, followed by 30 minutes of magnetic stirring. The resulting mixture was then transferred to a 100 mL Teflon-lined autoclave and heated to 140°C for 48 h. After the reaction, the product was washed several times with deionized water. The resulting bronze-colored precipitate was collected by centrifugation, washed several times with deionized water, and freeze-dried for 24 h to obtain the final NH<sub>4</sub>V<sub>4</sub>O<sub>10</sub> powder.

The cathode was prepared by mixing the NH<sub>4</sub>V<sub>4</sub>O<sub>10</sub> powder, Super P and PVDF with a mass ratio of 70:20:10 in NMP. The slurry was then coated on stainless steel meshes. After drying in oven at 60 °C for 12 h, the meshes with a mass ratio of 0.40-0.60 mg·cm<sup>-2</sup> were stamped into discs ( $\phi = 10$  mm) to be used as NH<sub>4</sub>V<sub>4</sub>O<sub>10</sub> cathodes.

### General Characterization

Fourier transform infrared (FT-IR) spectra of IIS were accessed with a Nicolet iS10 FT-IR spectrometer (Thermo Scientific, Waltham, USA), over a range of 500–4000 cm<sup>-1</sup> with a resolution of 4 cm<sup>-1</sup>. The chemical bonds of IIS were studied via a 4800X X-ray photoelectron spectroscopy (Thermo Fisher, Waltham, USA). The overlapping N peaks in the XPS profiles were deconvoluted into their individual components using Casa XPS software. Additionally, the element and chemical compositions of IIS were accessed by a Unicube Elementa (Elementar, Frankfurt, German), and a MesoMR23-060H-I solid state nuclear magnetic resonance (SSNMR) spectroscopy (Niumag, Suzhou, China). The crystalline structures were assessed by X-ray diffraction analysis, employing a DX-2700b X-ray diffractometer (XRD) (Haoyuan

Instrument, Dandong, China). The morphologies of the Zn@IIS and the bare zinc were studied using a Zeiss Crossbeam 350 scanning electron microscope (Zeiss, Oberkochen, Germany), assisted by a VK-X150 laser scanning confocal microscope (Keyence, Osaka, Japan).

### ***In-Situ* Raman Analysis**

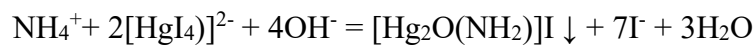
The electroplating process and zinc deposition behavior were monitored by an *in-situ* Raman spectroscopy (WITec Alpha-300, Oxford Instruments, Oxford, UK) at 50 mA·cm<sup>-2</sup>, combining with a BioLogical SP-150 electrochemical workstation (Biological France, Seyssinet-Pariset, France). The Raman laser was focused on the locally discharged zinc electrode, with a spectra center of 2300.00 cm<sup>-1</sup>, a laser wavelength of 532 nm, a laser intensity of 5.00, and 3 single spectra per 60 seconds.

### ***In-Situ* Optical Microscopy**

*In-situ* cycling progress was observed by ZEISS Lattice SIM 3 optical microscopy (ZEISS, Oberkochen, German) with a magnification of 4.5X at 10 mA·cm<sup>-2</sup> and 1mAh·cm<sup>-2</sup>, combined with the aforementioned SP-150 electrochemical workstation.

### **Qualitative Determination of Ammonium Ions**

Ammonium ions generated during the electroplating process were qualitatively determined using Nessler's reagent. [2] Briefly, 1.0 mL of Nessler's reagent was added to 25.0 mL of the electroplating solution after the formation of Zn@IIS. Subsequently, 2 M KOH was added dropwise until yellowish-brown flocculent precipitation appeared. The reaction of this test can be described as follows:



### **Bulk Property Measurements**

The porosity ( $P$ ) of Zn@IIS was calculated based on the following equation: [3]

$$P = \frac{\rho_a - \rho}{\rho_a} \times 100\% = \frac{\rho_a - \frac{m}{S \times \delta}}{\rho_a} \times 100\%$$

Where  $\rho_a$  is the actual density measured by a KC-120GY liquid densimeter (Cancham Instrument, Shanghai, China),  $\rho$  is the apparent density,  $m$  is the weight of IIS. The bottom area ( $S$ ) of the IIS layer corresponds to the area of the covered zinc foil, and the thickness ( $\delta$ ) of the IIS is determined by SEM images.

The contact angles of zinc anodes were measured using an OSA 100 contact angle goniometer (LAUDA Scientific, Lauda-Königshofen, German). The Young's modulus of Zn@IIS was measured using a TI-750L Hysitron Nanoindenter (Bruker, Billerica, USA) in an air-dried state.

### **Electrochemical Characterizations**

CR2032-type coin cells and glass fiber separators (GF/D) were used to evaluate coin cell performance at room temperature. Galvanostatic charge/discharge cycling was conducted using a CT-3001A battery testing system (Wuhan LAND Electronic Co. Ltd., Wuhan, China). The Zn||Zn symmetric cells were cycled in 2 M ZnSO<sub>4</sub> with the following parameters: 1 mA·cm<sup>-2</sup> and 1 mAh·cm<sup>-2</sup>, 5 mA·cm<sup>-2</sup> and 2 mAh·cm<sup>-2</sup>, 50 mA·cm<sup>-2</sup> and 10 mAh·cm<sup>-2</sup>, and 100 mA·cm<sup>-2</sup> and 2.5 mAh·cm<sup>-2</sup>. The Zn||Cu half-cells were cycled in 2 M ZnSO<sub>4</sub> at 5 mA·cm<sup>-2</sup> and 2 mAh·cm<sup>-2</sup>. Chronoamperometry (CA) curves were recorded using a CHI660E electrochemical workstation (CH Instruments Ins., Shanghai, China), with Zn||Zn symmetric cells monitored for 0-400 seconds in amperometry *i-t* curves. Electrochemical impedance spectroscopy (EIS) was performed on the aforementioned SP-150 electrochemical workstation, with frequency ranging from 0.01 to 100 kHz. The Zn||NH<sub>4</sub>V<sub>4</sub>O<sub>10</sub> full cells were cycled in 2 M ZnSO<sub>4</sub> within a voltage range of 0.2-1.6 V at current densities of 5 and 20 A·g<sup>-1</sup>, with rate performances measured at 5, 10, 15, 20, and 25 A·g<sup>-1</sup>. Cyclic voltammetry (CV) curves were obtained using the BioLogic SP-150 electrochemical workstation with a scanning rate of 0.1 mV s<sup>-1</sup>. For pouch cell evaluations, Zn||NH<sub>4</sub>V<sub>4</sub>O<sub>10</sub> cells were cycled in 2 M ZnSO<sub>4</sub> within a voltage range of 0.2-1.6 V at 1 A·g<sup>-1</sup>. The anodes comprised 20 μm, 3×2 cm<sup>2</sup> zinc foils, and the cathodes featured approximately 5 mg cm<sup>-2</sup> NH<sub>4</sub>V<sub>4</sub>O<sub>10</sub> on 3×2 cm<sup>2</sup> stainless steel meshes.

Linear scanning voltammetry (LSV) curves were recorded using the CHI660E electrochemical workstation with a three-electrode system (working electrode: zinc foil, counter electrode: platinum foil, reference electrode: Ag/AgCl). The measurements were conducted between -2.0 and -1.2 V with a scan rate of 5 mV s<sup>-1</sup> in a 2 M Na<sub>2</sub>SO<sub>4</sub> solution. Tafel plot tests were also performed on the CHI660E electrochemical workstation using the same three-electrode setup. These tests were conducted between -1.1 and -0.9 V with a scan rate of 0.1 mV s<sup>-1</sup> in a 2 M ZnSO<sub>4</sub> solution.

### Determination of Transference Number of $Zn^{2+}$ ( $t_{Zn^{2+}}$ )

The transference number of  $Zn^{2+}$  ( $t_{Zn^{2+}}$ ) was measured in Zn||Zn symmetric cells. This calculation was based on chronopotentiometry (CA) curves obtained with 10 mV polarization voltage for 5000 s and electrochemical impedance spectroscopy (EIS) curves recorded before and after polarization. The formula used is as follows: [4]

$$t_{Zn^{2+}} = \frac{I_s(\Delta V - I_0 R_0)}{I_0(\Delta V - I_s R_s)}$$

Where  $\Delta V$  represents the polarization voltage (10 mV),  $I_0$  and  $I_s$  correspond to the current (mA) at the initial and steady states, respectively.  $R_0$  and  $R_s$  denote the interfacial resistances ( $\Omega$ ) between the electrolyte and electrode at the initial and steady states, respectively.

### Determination of $Zn^{2+}$ Conductivity ( $\sigma$ )

The  $Zn^{2+}$  conductivity ( $\sigma$ ) was determined using Ti||Ti and IIS (pressed on the Ti foil) ||Ti symmetric cells in a 2 M  $ZnSO_4$  solution. This calculation was based on Nyquist plots recorded over a frequency range from 0.1 to 100k Hz. The formula used is as follows: [5]

$$\sigma = \frac{L}{R_b S}$$

Where  $R_b$  represents the ohmic resistance obtained from the intersection of the EIS curve with the x-axis,  $L$  is the thickness of the IIS layer pressed onto the Ti foil, and  $S$  is the contact area between the electrode and electrolyte. Additionally, conductivity measurements were performed using a double-testing digital four-probe tester (ST2263, Jingge, Nanjing, China).

### Simulations

The first principles calculation in this work was performed in the framework of Density Functional Theory (DFT). The Vienna *Ab-initio* Simulation Package (VASP) was firstly adopted for geometry optimization and electronic property investigation, with Projector Augmented Wave (PAW) method applied to solve the Kohn-Sham equations and Generalized Gradient Approximation (GGA) constructed by Perdew-Burke-Ernzerhof (PBE) taken as exchange-correlation energy functional. Considering

that the phase transformation during the *in-situ* excitation process occurs in aqueous solution, the reaction enthalpy was computed using an implicit solvation model (VASPsol) after obtaining the optimized structures. Moreover, the orbital properties as well as the electrostatic potentials of the investigated models were revealed using DMol. All the calculation tasks were conducted at the cutoff energy of 480 eV in a  $\Gamma$ -centered  $k$ -grid scheme with a total number of 40, during which process the convergence criteria were set to be  $10^{-4}$  eV for energy and  $10^{-2}$  eV/Å for force.

The distribution of electric fields and ion fluxes at the electrode-anode interface was predicted using a 2D Nernst-Planck formulation that accounts for both diffusion and migration in the bulk electrolyte and electrode, as shown below: <sup>[6]</sup>

$$\nabla^2 \phi = -F \sum z_i C_i$$

$$\frac{\partial C_i}{\partial t} = \nabla \cdot \left[ D_i \nabla C_i + \frac{D_i C_i}{RT} z_i \nabla \phi \right]$$

Where  $F$ ,  $R$ , and  $T$  represent the Faraday constant, ideal gas constant, and temperature, respectively.  $D_i$  is the diffusion coefficient ( $0.703 \times 10^{-9}$  m<sup>2</sup>/s for Zn<sup>2+</sup>),  $C_i$  is the concentration,  $z_i$  is the charge number, and  $\phi$  is the electrolyte potential. Electroneutrality is assumed throughout the domains. In the experiment, the flux of zinc ions is uniform through the initial structure. The electrode length is 25  $\mu\text{m}$ , and the overall diffusion distance of the electrolyte is 20  $\mu\text{m}$ .

For the case without a solid electrolyte interphase (SEI) (IDA-Zn), a model with a semicircle and initial structure is established to determine the electric field distribution in various deposition states. Next, for the semicircle structure with SEI (IDA-Zn), which is randomly distributed on the zinc anodes, the evolution of the electric field distribution in different deposition states is considered. For the case without SEI (IDA-Zn), a model with a semicircle and initial structure is used to determine the zinc ion flux in different deposition states. For the semicircle structure with SEI (IDA-Zn), which is also randomly distributed on the zinc anodes, the evolution of zinc ion flux in various deposition states is evaluated. The electrochemical model was imported into the finite element software COMSOL<sup>®</sup> (Stockholm, Sweden), where material properties were defined, and relevant problems were calculated and analyzed. The Parallel Direct Sparse Solver (PARDISO) was employed to solve the discretized

transport and electrode deformation kinematics equations, and time stepping was handled using second-order backward Euler differentiation.

## Supporting Information

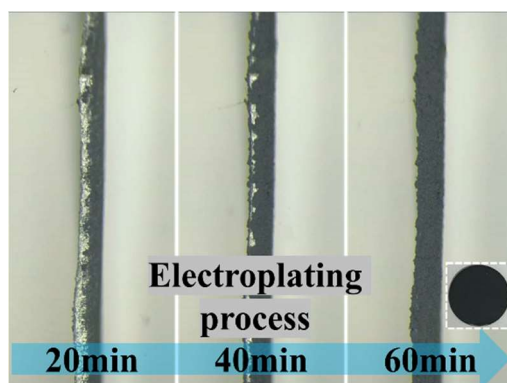


**Figure S1.** *In-situ* cross-sectional optical microscopy image of the zinc anode during charging and discharging at  $10 \text{ mA}\cdot\text{cm}^{-2}$  and  $1 \text{ mAh}\cdot\text{cm}^{-2}$  in  $2 \text{ M ZnSO}_4 + 5 \text{ g}\cdot\text{L}^{-1}$  IDAN.

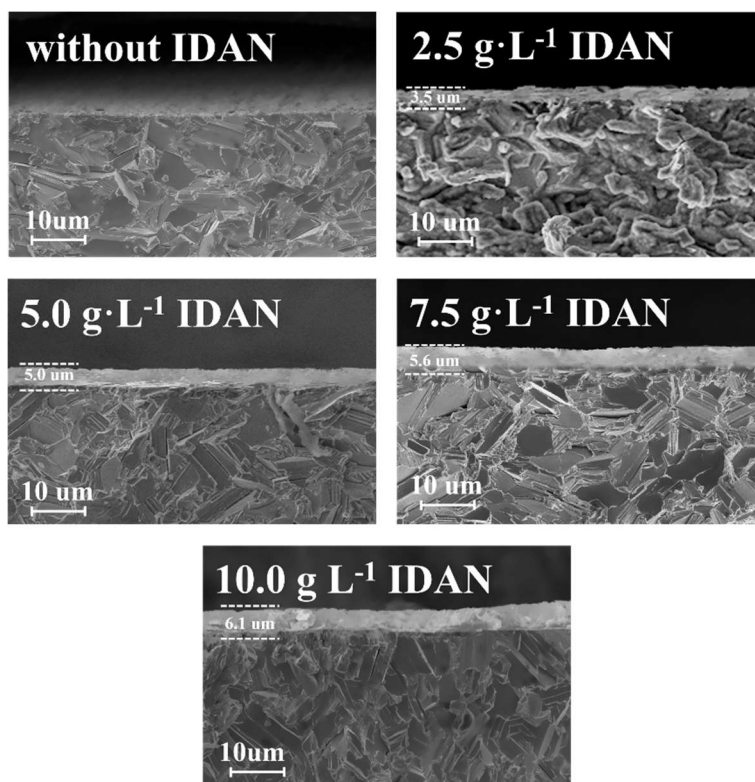


**Figure S2.** The SEM images for cross section of Zn anodes covered by SEI layer with various thickness derived by 0, 2.5, 5.0, 7.5, and  $10.0 \text{ g}\cdot\text{L}^{-1}$  IDAN.

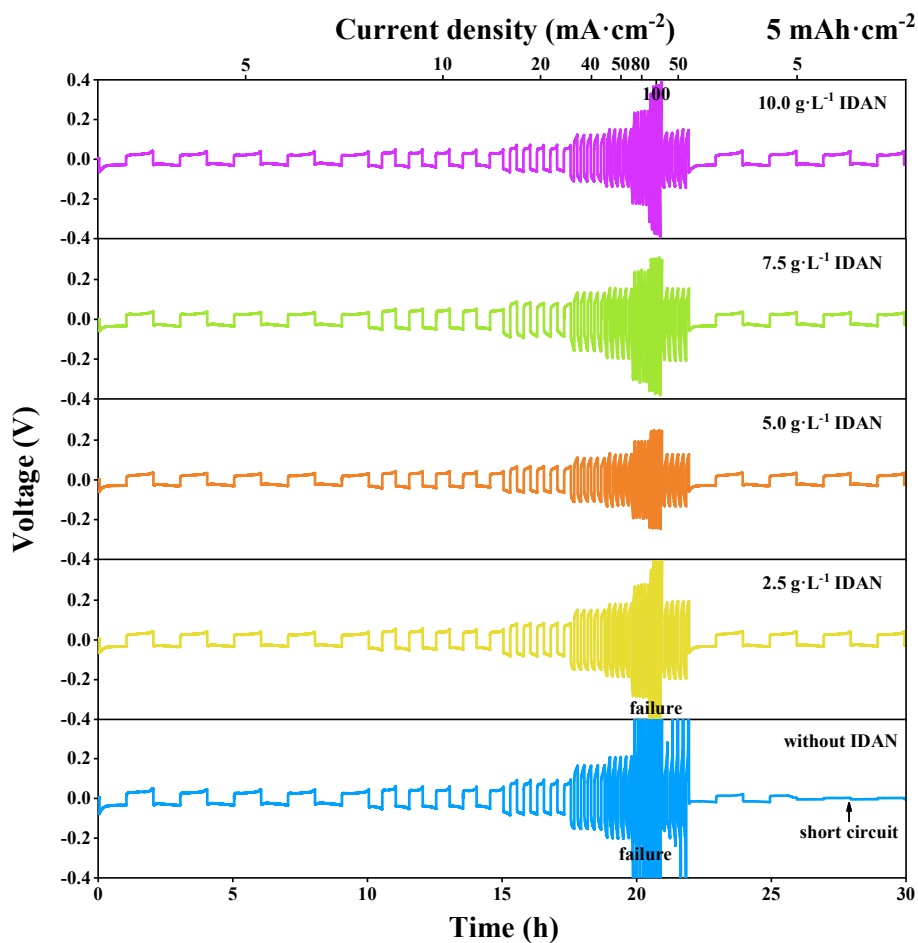


**Figure S3.** Rate cycling performances of the zinc electrode after electroplating ( $50 \text{ mA}\cdot\text{cm}^{-2}$ , 120 s) in  $2 \text{ M ZnSO}_4$  with 0, 2.5, 5.0, 7.5, and  $10.0 \text{ g}\cdot\text{L}^{-1}$  IDAN under current densities of 5, 10, 20, 40, 50, 80, and  $100 \text{ mA}\cdot\text{cm}^{-2}$  with an area capacity of  $5 \text{ mAh}\cdot\text{cm}^{-2}$ .

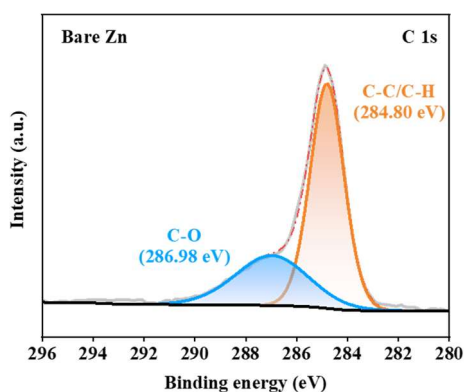


**Figure S4.** C 1s XPS analysis of bare zinc extracted from symmetric cells after the rate cycling tests.

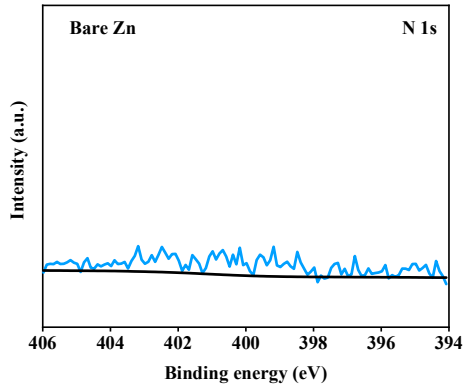


**Figure S5.** N 1s XPS analysis of bare zinc extracted from symmetric cells after the rate cycling tests.

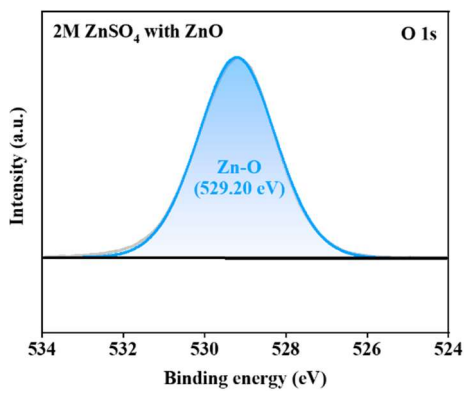


**Figure S6.** O 1s XPS analysis of ZnO generated in 2 M ZnSO<sub>4</sub>.

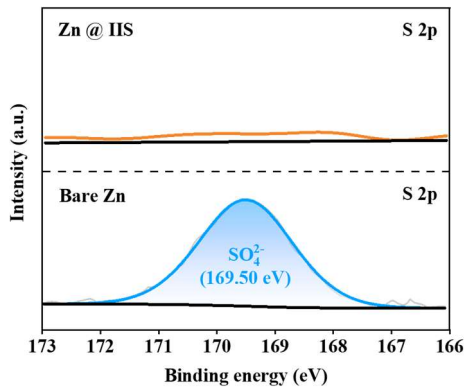


**Figure S7.** S 2p XPS analysis of Zn@IIS and bare zinc extracted from symmetric cells after the rate cycling tests.

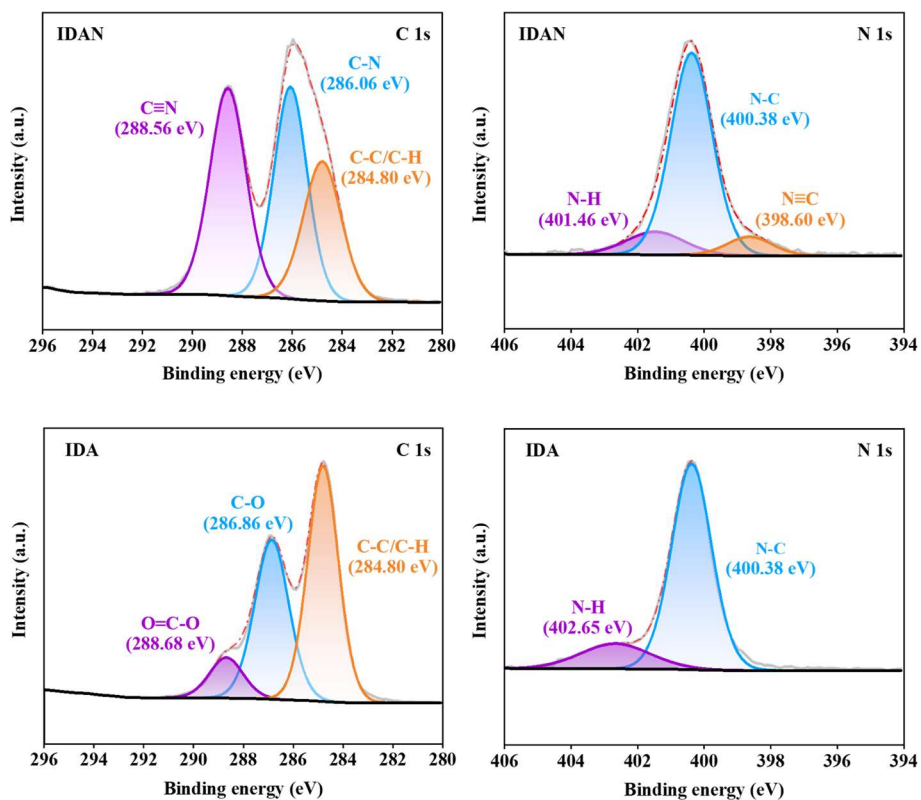


Figure S8. XPS spectrum of standard IDAN and IDA samples.

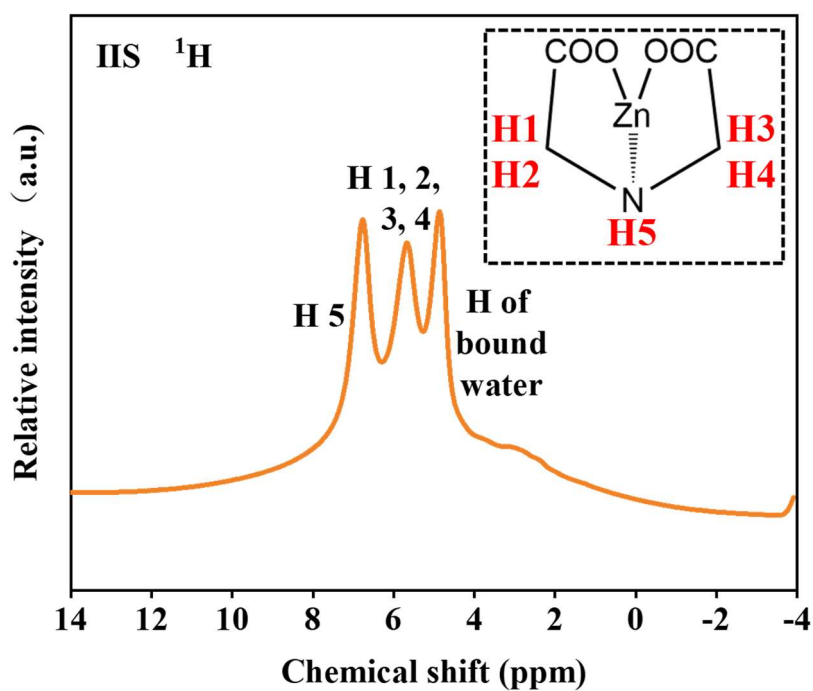
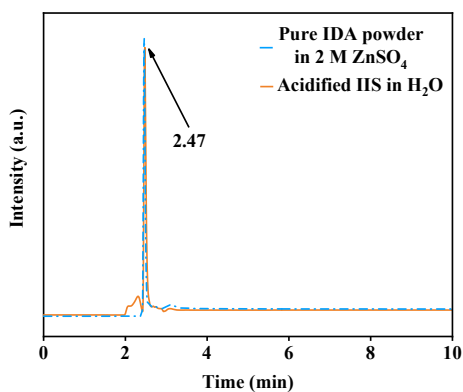


Fig S9. <sup>1</sup>H SSNMR of IIS scratched from zinc foils.



**Figure S10.** Precipitation phenomena observed in the electroplating solution with IDAN additives (left) and without IDAN (right) after the addition of Nessler's reagent. The presence of yellowish-brown flocculent precipitates in the solution with IDAN indicates ammonium ion generation, while no significant change is noted in the solution without IDAN.



**Figure S11.** High-Performance Liquid Chromatography of Acidified IIS in  $\text{H}_2\text{O}$  and pure IDA powder in 2 M  $\text{ZnSO}_4$ .

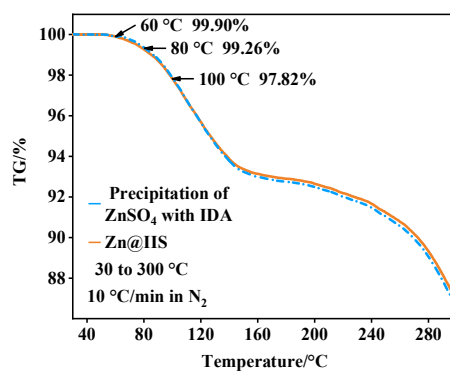


**Figure S12.** Thermal Gravimetric Analysis of  $\text{Zn@IIS}$  and precipitation of 2 M  $\text{ZnSO}_4$  solution added into 2 M IDA solution.



**Figure S13.** The conductivity of the Zn@IIS and the bare zinc foil.

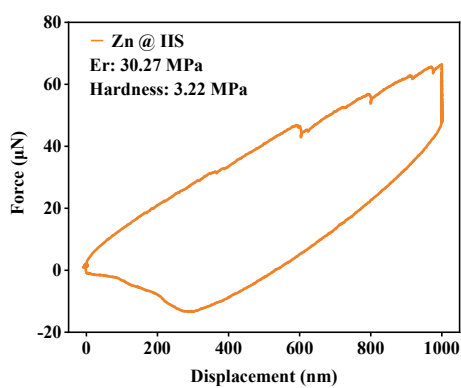


**Figure S14.** Nano-scratch tests of the Zn@IIS.

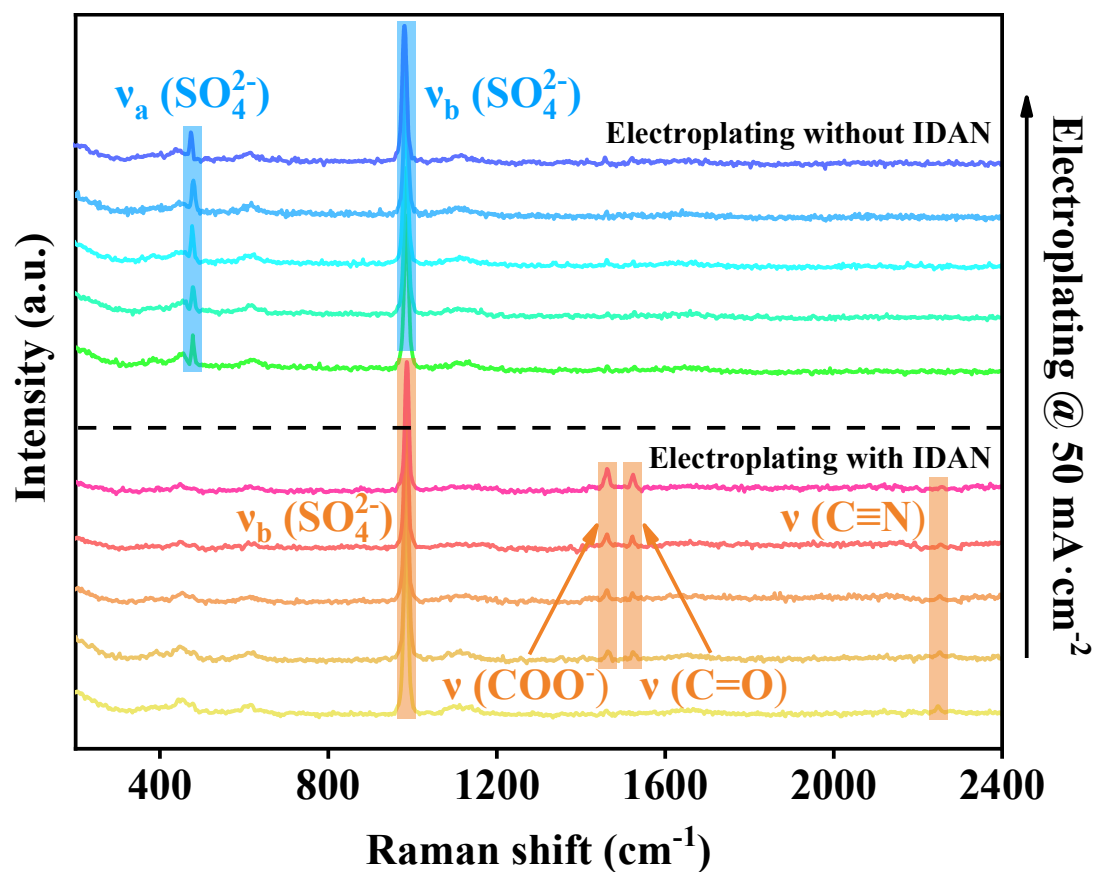


**Figure S15.** *In-situ* Raman spectroscopy of electroplating at  $50 \text{ mA}\cdot\text{cm}^{-2}$  in  $2 \text{ M ZnSO}_4$  with/without IDAN, ranging from  $200$  to  $2400 \text{ cm}^{-1}$ , with one scanning per two minutes.

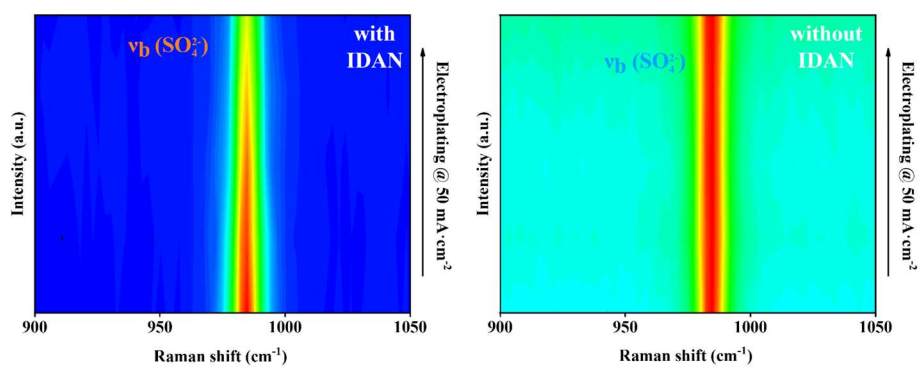


**Figure S16.** *In-situ* Raman spectroscopy of electroplating at  $50 \text{ mA}\cdot\text{cm}^{-2}$  in  $2 \text{ M ZnSO}_4$  with/without IDAN, focusing on the sulfate, with one scanning per minute.

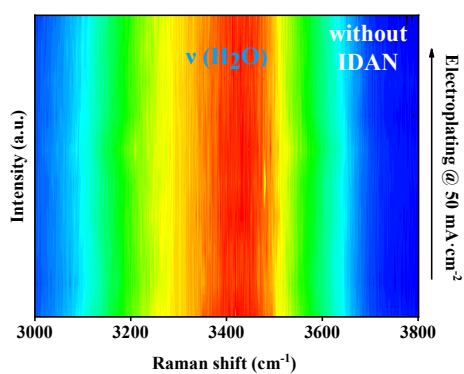


**Figure S17.** *In-situ* Raman spectroscopy of electroplating at  $50 \text{ mA}\cdot\text{cm}^{-2}$  in  $2 \text{ M ZnSO}_4$  without IDAN, focusing on the water, with one scanning per minute.

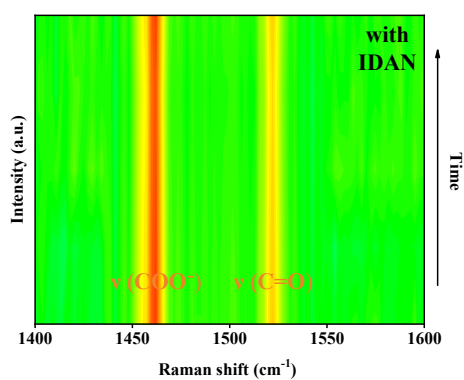


**Figure S18.** *In-situ* Raman spectroscopy for supplementary 24 hours after electroplating, focusing on the carboxyl group, with one scanning per hour.

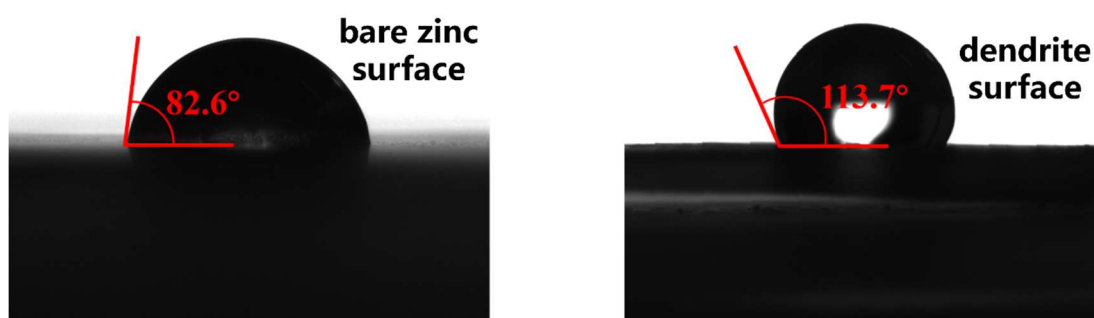


**Figure S19.** The contact angles of the bare zinc foil and the zinc foil with a dendrite surface after cycling at a current density of  $10 \text{ mA}\cdot\text{cm}^{-2}$  with an area capacity of  $1 \text{ mAh}\cdot\text{cm}^{-2}$  for 60 minutes.

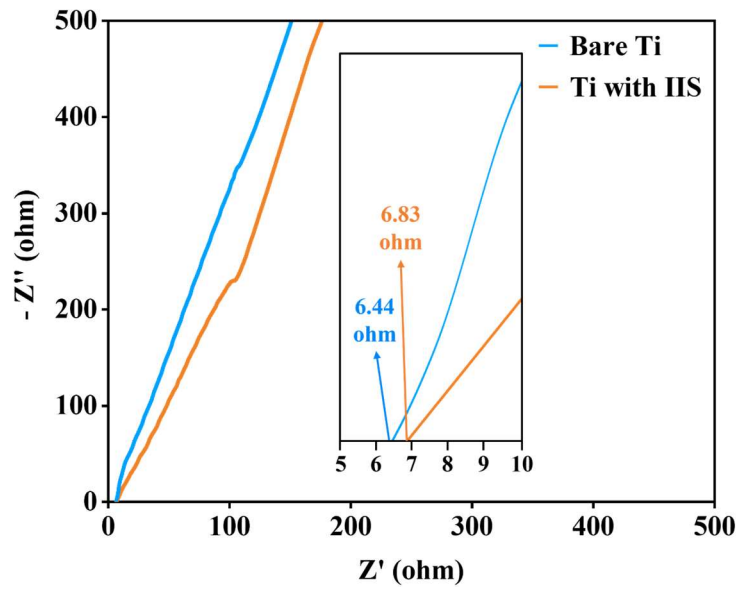


**Figure S20.** Nyquist plots of Ti||Ti and IIS (pressed on the Ti foil)||Ti symmetric cells in 2 M ZnSO<sub>4</sub>.

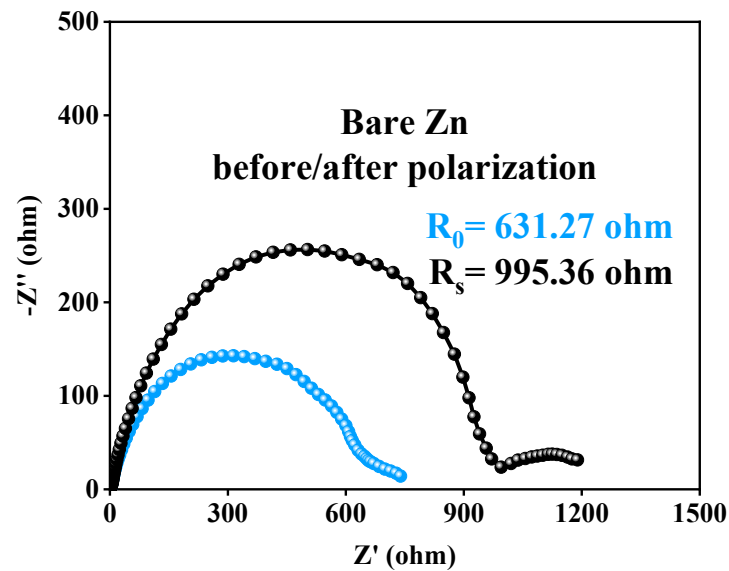


**Figure S21.** EIS before and after polarization of Zn||Zn symmetric cells of bare zinc in 2M ZnSO<sub>4</sub>.

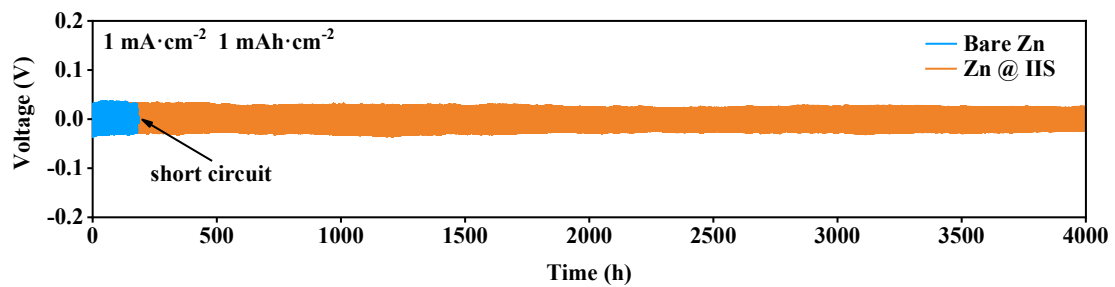


**Figure S22.** Long-term cycling performance of Zn||Zn symmetric cells in 2 M ZnSO<sub>4</sub> at a current density of 1 mA·cm<sup>-2</sup> with an area capacity of 1 mAh·cm<sup>-2</sup>.

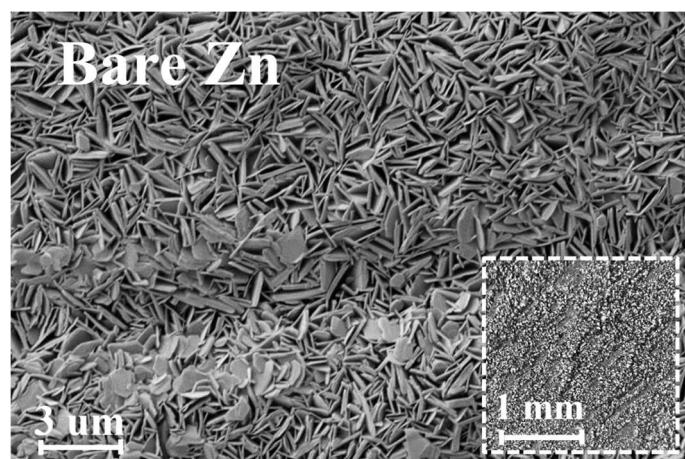


**Fig S23.** SEM image of bare zinc after the cycling at a current density of  $5 \text{ mA} \cdot \text{cm}^{-2}$  with an area capacity of  $2 \text{ mAh} \cdot \text{cm}^{-2}$ .

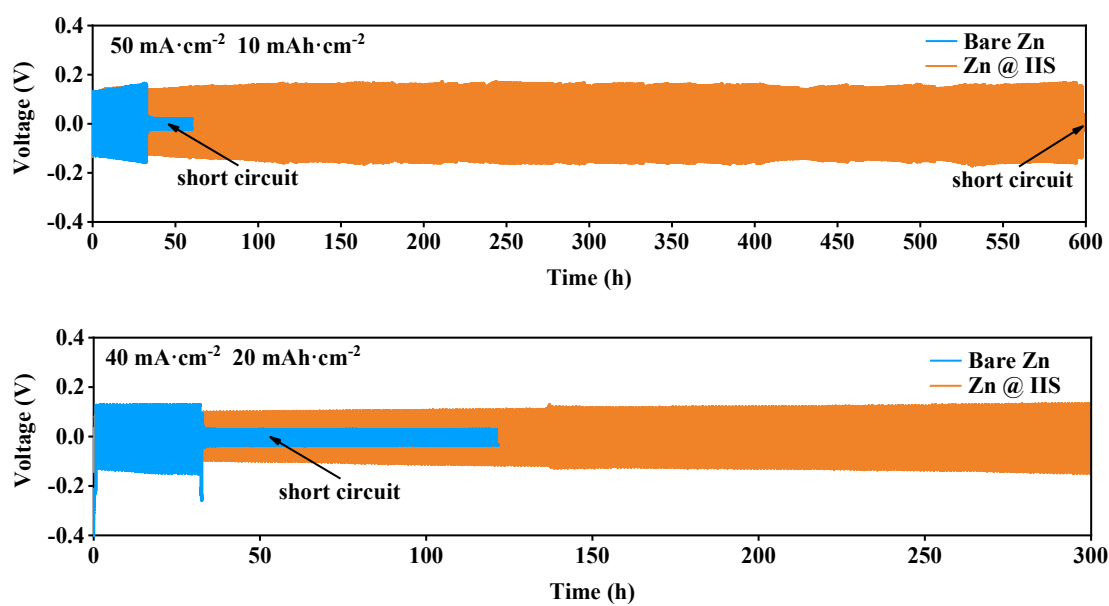


**Figure S24.** Cycling performance of Zn||Zn symmetric cells in 2 M ZnSO<sub>4</sub> at a current density of  $50 \text{ mA} \cdot \text{cm}^{-2}$  with an area capacity of  $10 \text{ mAh} \cdot \text{cm}^{-2}$  and a current density of  $40 \text{ mA} \cdot \text{cm}^{-2}$  with an area capacity of  $20 \text{ mAh} \cdot \text{cm}^{-2}$ .

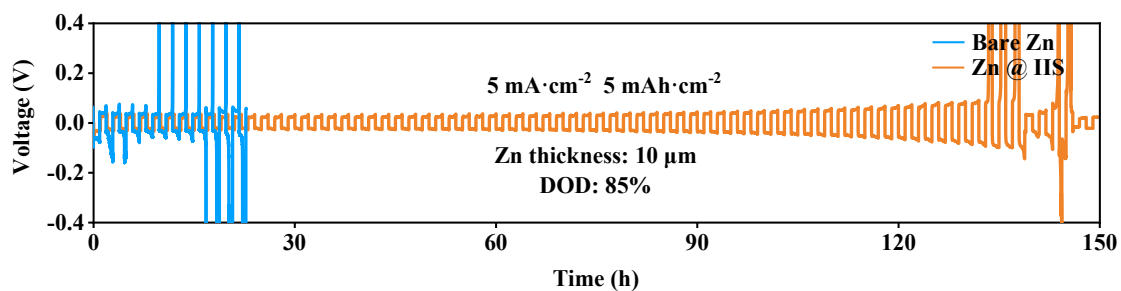


**Figure S25.** Cycling performance of Zn||Zn symmetric cells in 2 M ZnSO<sub>4</sub> under an 85% depth of discharge and a current density of 5.0 mA·cm<sup>-2</sup>.

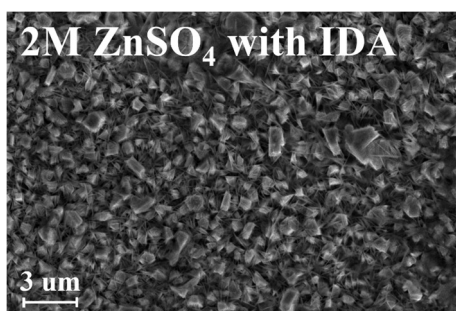
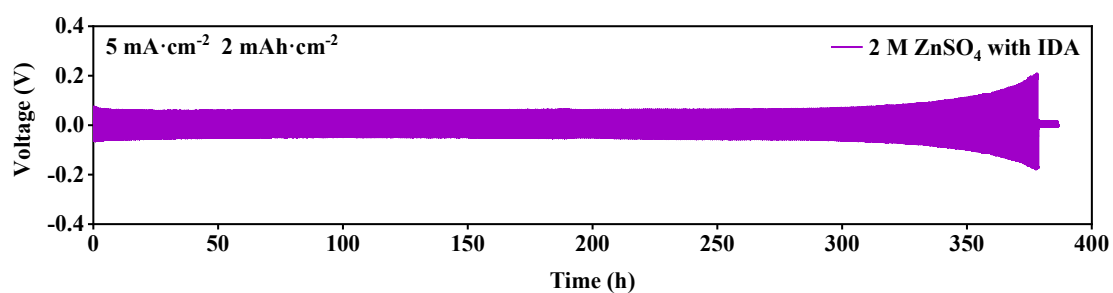


**Figure S26.** The cycling performance and the anode morphology of the IDA-added Zn||Zn symmetric cells at a current density of 5 mA·cm<sup>-2</sup> with an area capacity of 2 mAh·cm<sup>-2</sup>.

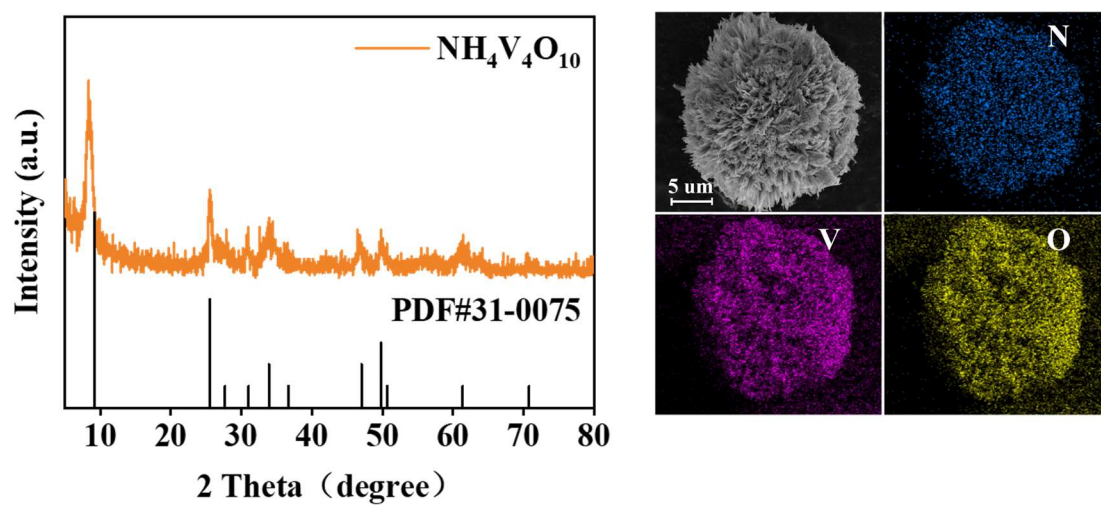


**Figure S27.** XRD pattern and SEM-EDS images of the NH<sub>4</sub>V<sub>4</sub>O<sub>10</sub> powder.

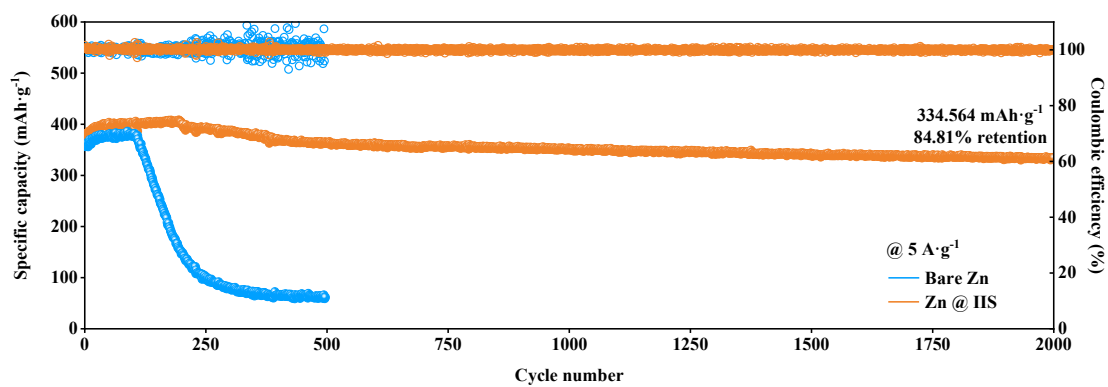


**Figure S28.** Long-term cycling performance of Zn||NH<sub>4</sub>V<sub>4</sub>O<sub>10</sub> full cells in 2 M ZnSO<sub>4</sub> at 5 A·g<sup>-1</sup>.

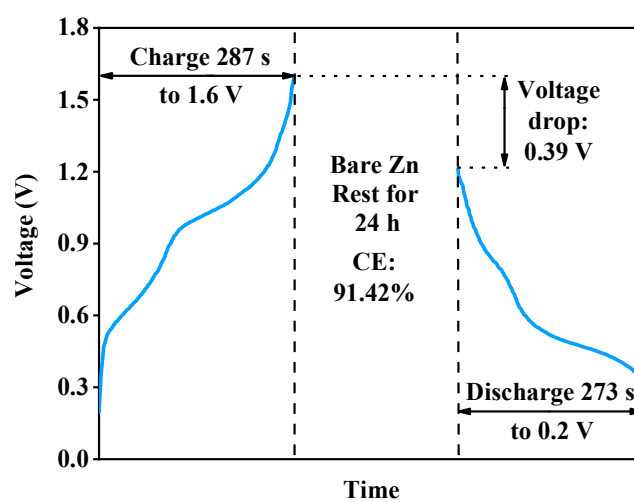


**Figure S29.** Capacity retention of Zn||NH<sub>4</sub>V<sub>4</sub>O<sub>10</sub> full cells of bare zinc after charging to 1.6 V, resting for 24 h and discharging to 0.2 V.

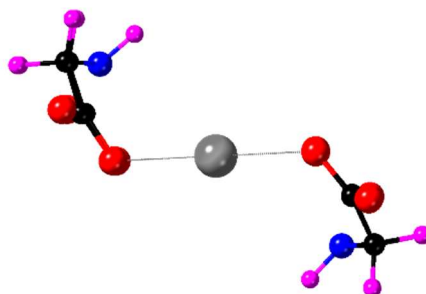


**Figure S30.** Long-range diffusion: coordinate (axis b) of N1 and N2: 0.25, 0.75.

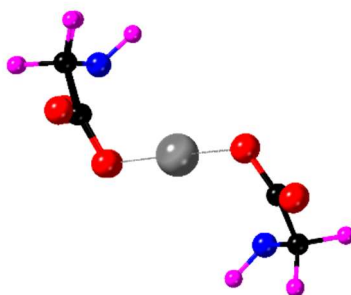


**Figure S31.** Short-range diffusion: coordinate (axis b) of N1 and N2: 0.35, 0.65.

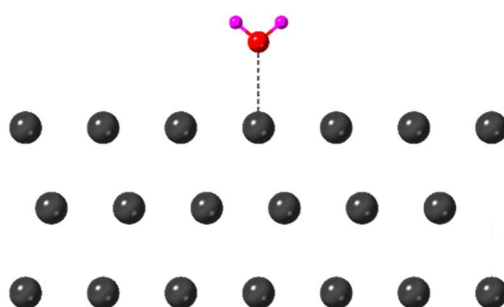


**Figure S32.** Adsorption of H<sub>2</sub>O on Zn (001): Zn-O bond length is 2.53 Å, with an energy of -2.08 eV.

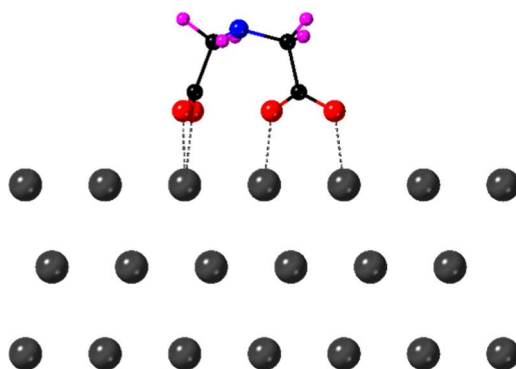


**Figure S33.** Adsorption of IDA on Zn (001): Zn-O bond length is 2.14 Å, with an energy of -5.62 eV.

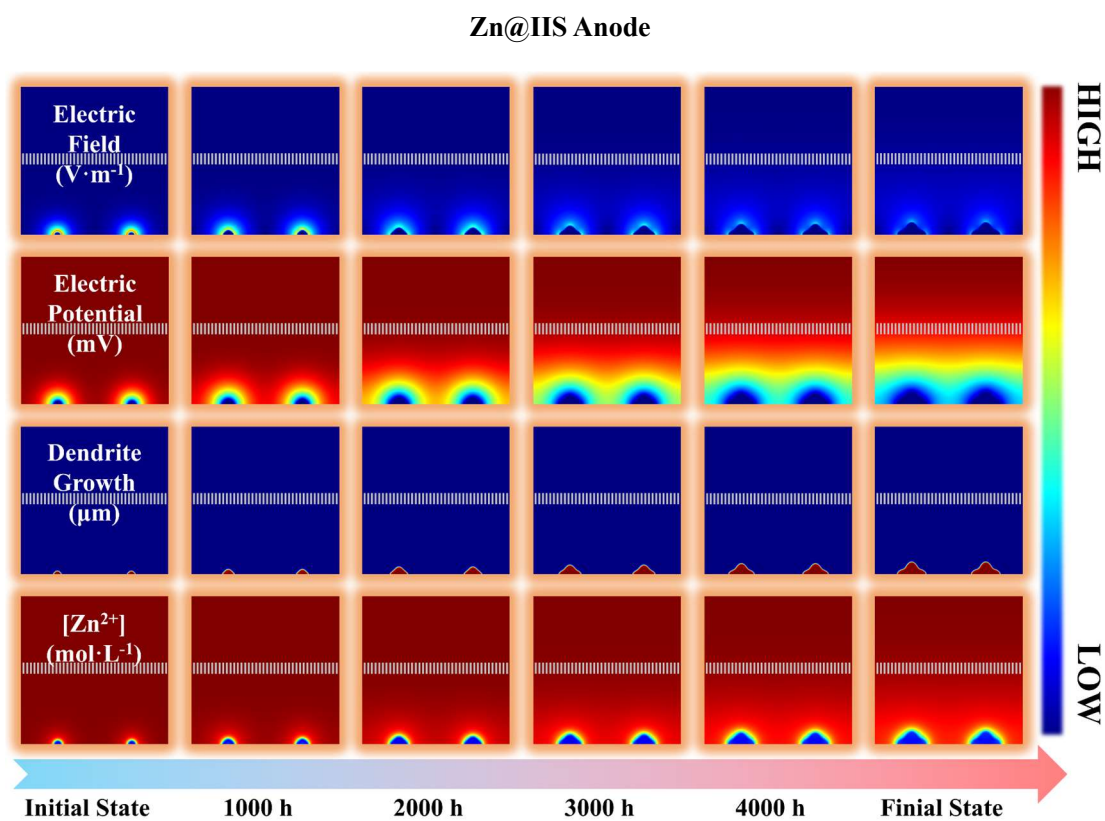
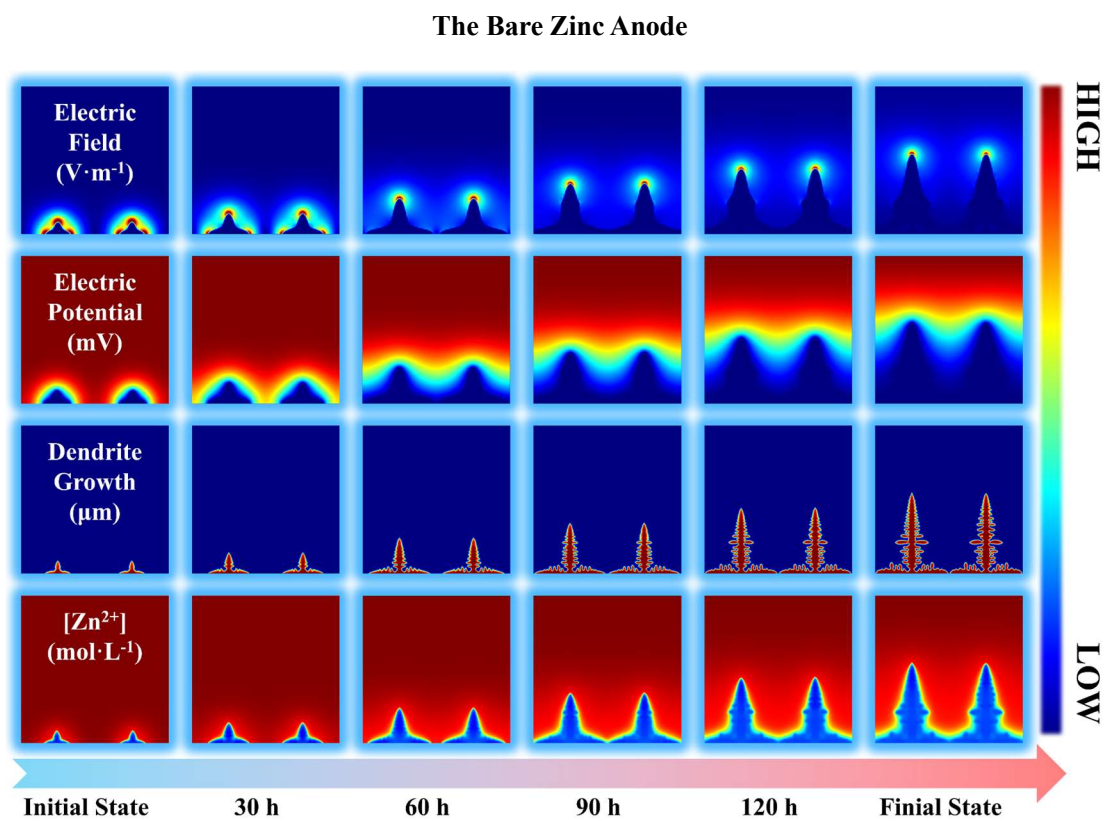


**Figure S34.** Finite element simulation of zinc anode in Zn||Zn symmetric cell related to the above cycling ( $5 \text{ mA}\cdot\text{cm}^{-2}$ ,  $2 \text{ mAh}\cdot\text{cm}^{-2}$ ), 120 hours for bare zinc and 4000 hours for Zn@IIS, including electric field, electric potential, dendrite growth and zinc ions flux.

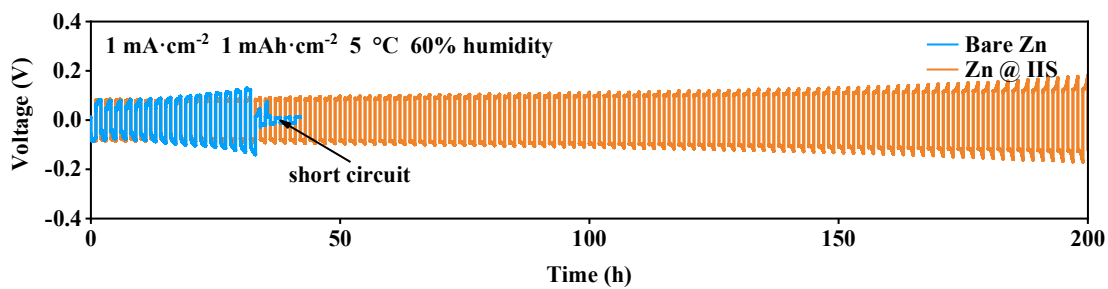
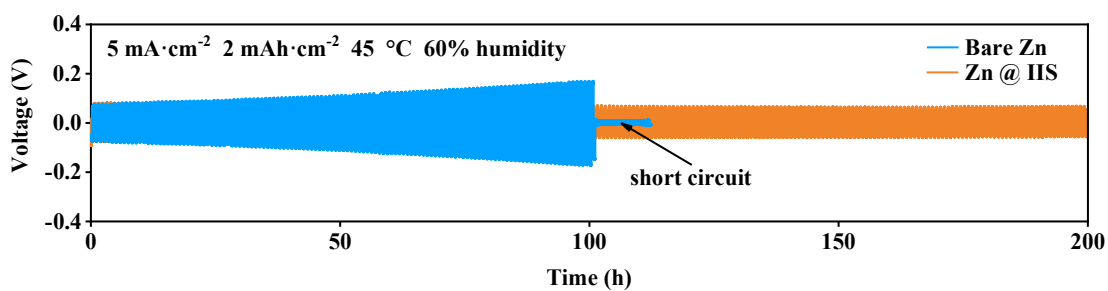


**Figure S35.** Cycling performance of Zn||Zn symmetric cells in 2 M ZnSO<sub>4</sub> under 5 °C and 45 °C in 60% relative humidity.

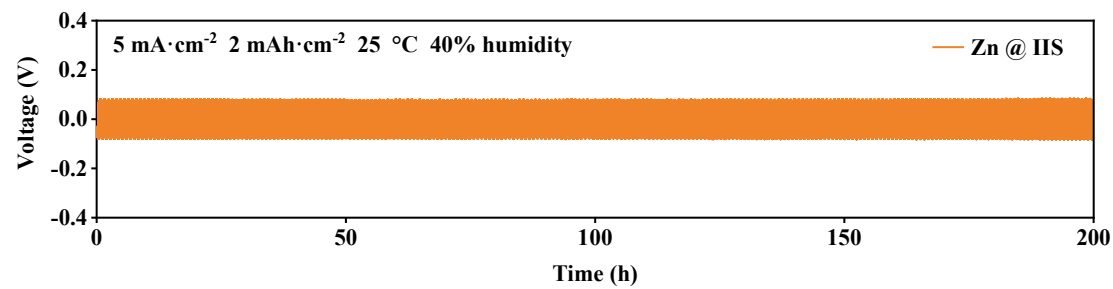
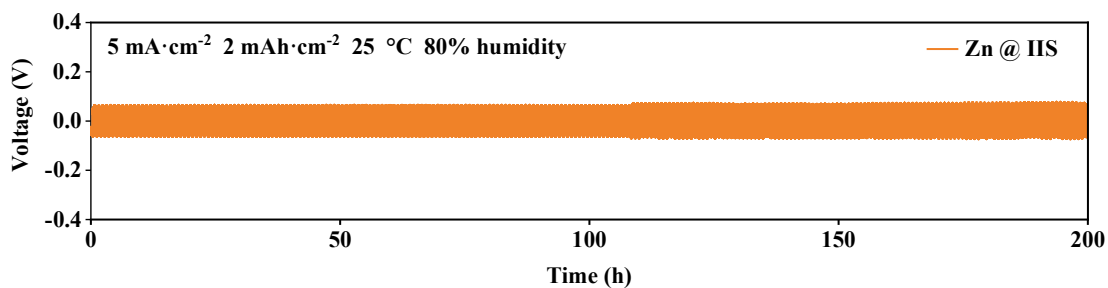


**Figure S36.** Cycling performance of Zn||Zn symmetric cells in 2 M ZnSO<sub>4</sub> under 40% and 80% relative humidity in 25 °C.

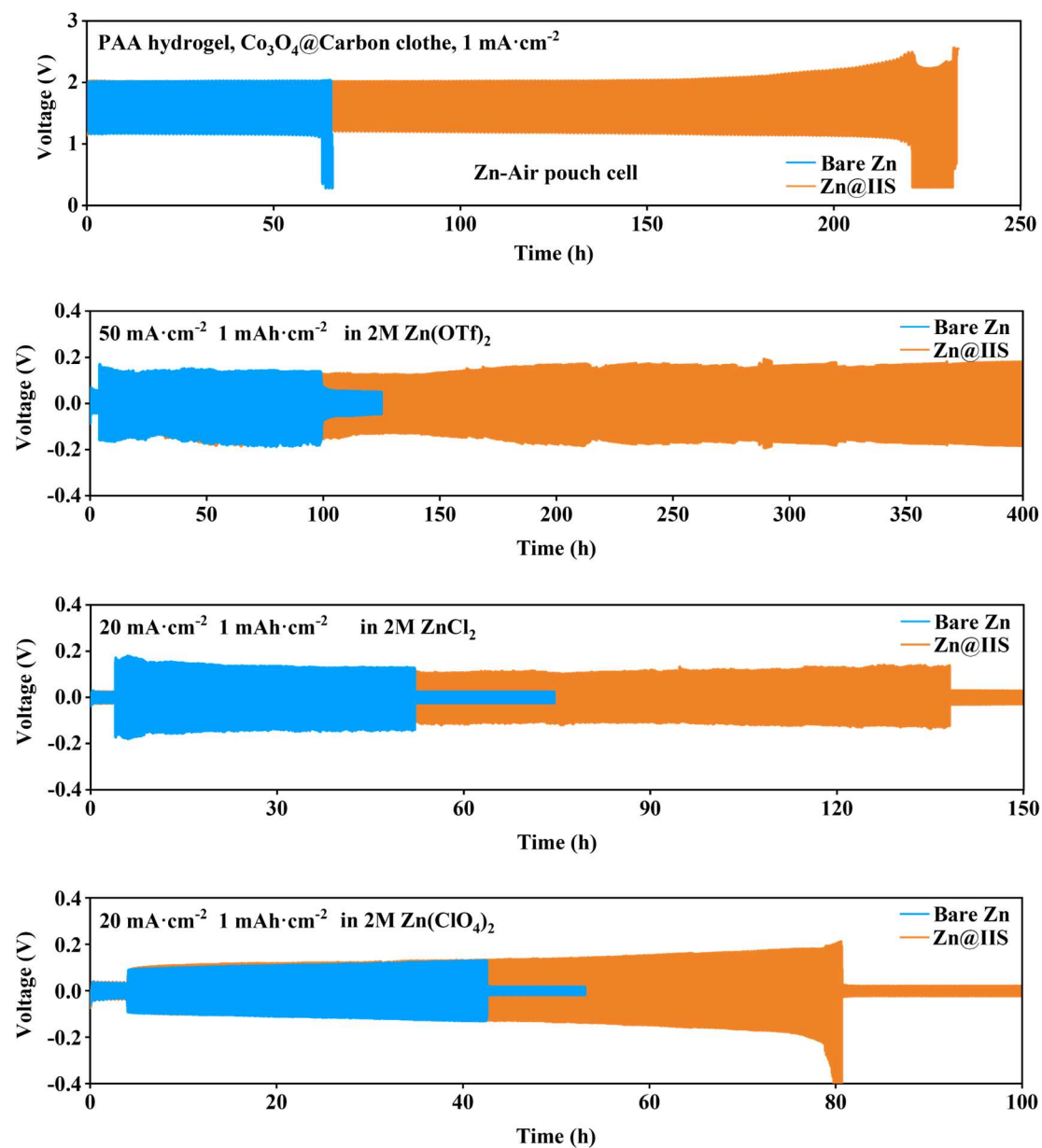


**Figure S37.** Cycling performance of Zn-Air pouch cells, Zn||Zn symmetric cells in 2 M Zn(OTf)<sub>2</sub>, Zn||Zn symmetric cells in 2 M ZnCl<sub>2</sub> and Zn||Zn symmetric cells in 2 M Zn(ClO<sub>4</sub>)<sub>2</sub> using bare zinc and Zn@IIS as anodes.

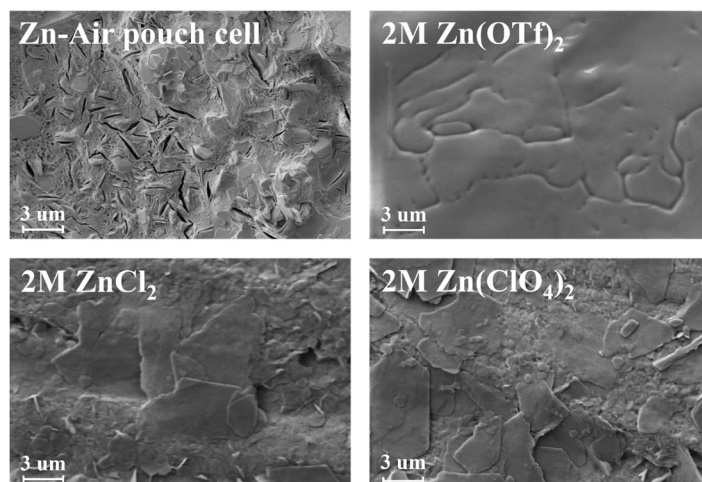


**Figure S38.** SEM images for the Zn@IIS morphologies of Zn-Air pouch cells, Zn||Zn symmetric cells in 2 M Zn(OTf)<sub>2</sub>, Zn||Zn symmetric cells in 2 M ZnCl<sub>2</sub> and Zn||Zn symmetric cells in 2 M Zn(ClO<sub>4</sub>)<sub>2</sub>.

**Table S1.** Ion chromatography of  $\text{NH}_4^+$  and  $\text{IDA}^{2-}$  in the electrolyte after IDAN-added electrodeposition.

Ion Chromatography (Initial)					
Ions	Concentration $\text{mg}\cdot\text{L}^{-1}$	Volume mL	Mass mg	Molar Mass $\text{g}\cdot\text{mol}^{-1}$	Amount mmol
$\text{NH}_4^+$	146.1028	10.0135	1.4630	18.04	0.0811
$\text{NH}(\text{CH}_2\text{COO}^-)_2$	415.0384	10.0135	4.156	131.1	0.0317

Ion Chromatography (After 24h)					
Ions	Concentration $\text{mg}\cdot\text{L}^{-1}$	Volume mL	Mass mg	Molar Mass $\text{g}\cdot\text{mol}^{-1}$	Amount mmol
$\text{NH}_4^+$	147.1046	10.0194	1.4739	18.04	0.0817
$\text{NH}(\text{CH}_2\text{COO}^-)_2$	418.9910	10.0194	4.198	131.1	0.0320

**Table S2.** BET tests for the anode surface after the zinc deposition.

Deposited Zn Surface	Surface Area $\text{m}^2\cdot\text{g}^{-1}$	Pore Volume $\text{cm}^3\cdot\text{g}^{-1}$
In ZnSO4	29.1593	0.0094
In ZnSO4 with IDA	19.6342	0.0074
In ZnSO4 IIS	0.2740	0.0008

## References

- 1 H. Zhang, Y. Zhong, J. Li, Y. Liao, J. Zeng, Y. Shen, L. Yuan, Z. Li and Y. Huang, Inducing the Preferential Growth of Zn (002) Plane for Long Cycle Aqueous Zn-Ion Batteries, *Adv. Energy Mater.*, 2023, **13**, 2203254.
- 2 X. Gao, Y. Wen, D. Qu, L. An, S. Luan, W. Jiang, X. Zong, X. Liu and Z. Sun, Interference Effect of Alcohol on Nessler's Reagent in Photocatalytic Nitrogen Fixation, *ACS Sustain. Chem. Eng.*, 2018, **6**, 5342-5348.
- 3 W. Liu, M. Kappl and H. Butt, Tuning the Porosity of Supraparticles, *ACS Nano*, 2019, **13**, 13949-13956.
- 4 Z. Zha, T. Sun, D. Li, T. Ma, W. Zhang and Z. Tao, Zwitterion as electrical double layer regulator to in-situ formation of fluorinated interphase towards stable zinc anode, *Energy Storage Mater.*, 2024, **64**, 103059.
- 5 M. Liu, W. Yuan, G. Ma, K. Qiu, X. Nie, Y. Liu, S. Shen and N. Zhang, In-Situ Integration of a Hydrophobic and Fast-Zn<sup>2+</sup>-Conductive Inorganic Interphase to Stabilize Zn Metal Anodes, *Angewandte Chemie International Edition*, 2023, **62**, e202304444.
- 6 B. Liu, C. Wei, Z. Zhu, Y. Fang, Z. Bian, X. Lei, Y. Zhou, C. Tang, Y. Qian and G. Wang, Regulating Surface Reaction Kinetics through Ligand Field Effects for Fast and Reversible Aqueous Zinc Batteries, *Angewandte Chemie International Edition*, 2022, **61**, e202212780.